Chemical Science

Accepted Manuscript

This article can be cited before page numbers have been issued, to do this please use: L. Chen, L. Zhang, Z. Chen, H. Liu, R. Luque and Y. Li, *Chem. Sci.*, 2016, DOI: 10.1039/C6SC01659F.

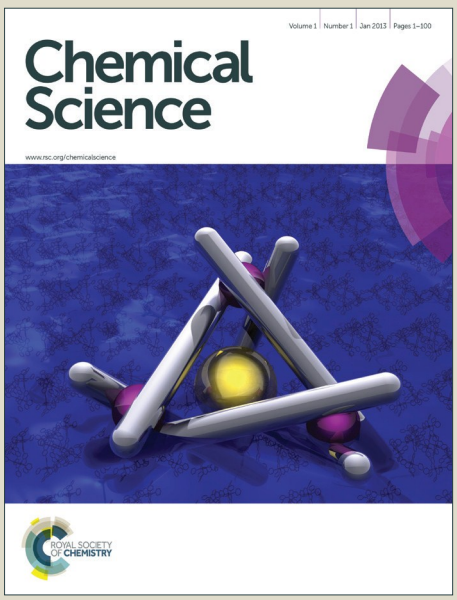

ROYAL SOCIETY OF CHEMISTRY

www.rsc.org/chemicalscience

View Article Online
DOI: 10.1039/C6SC01659F

Journal Name

ARTICLE

A covalent organic framework-based route to *in-situ* encapsulation of metal nanoparticles in *N*-rich hollow carbon spheres

Received 00th January 20xx,
Accepted 00th January 20xx

DOI: 10.1039/x0xx00000x

www.rsc.org/

Liyu Chen,[a] Lei Zhang,[a] Zhijie Chen,[a] Hongli Liu,[a] Rafael Luque,*[b] and Yingwei Li*[a]

Metal nanoparticles (NPs) encapsulated in hollow nanostructures hold great promise for a variety of applications. Herein, we demonstrate a new concept that covalent organic frameworks (COFs) doped with metal cations can be readily used as novel precursors for in-situ encapsulation of metal NPs into N doped hollow carbon spheres (NHCS) through a controlled carbonization process. The obtained Pd@NHCS composites show significantly enhanced catalytic activity and selectivity in the hydrogenation of nitrobenzene in ethanol and oxidation of cinnamyl alcohol compared with that of conventional Pd/N-C and commercial Pd/C catalysts. The excellent catalytic performance should be related to the synergism of porous hollow spheric structure, highly dispersed Pd NPs, and uniform distribution of N dopants on the materials. We believe this newly developed methodology could be extended to the synthesis of other metal NPs@NHCS composites for a variety of advanced applications.

Introduction

Hollow-structured porous materials, with large internal voids and porous shells, have promising applications in a variety of fields, such as gene therapy, confined catalysis, adsorption and storage.[1] Among such systems, hollow carbon spheres (HCS) are very attractive owing to their outstanding features of low density, good thermal stability, and high permeability.[2] Recently, considerable interests have been raised to employ HCS as nanoreactors by encapsulating catalytically active metal nanoparticles (NPs) in the porous shell of HCS.[3] The shell could function as a barrier to prevent encapsulated metal NPs from coalescence, and the pore in the shell connecting the hollow core can provide a highway network for the free diffusion of reactant molecules to access the metal active sites.[4] Moreover, it has been demonstrated that incorporation of heteroatoms (e.g., nitrogen, boron, sulphur and phosphorus) into the carbon lattice can significantly improve its chemical and electrical properties, and also enhance the interactions between the carbon support and the embedded metal NPs to trigger superior catalytic performance.[5]

Considerable efforts have been devoted to exploring effective strategies for the preparation of metal NPs encapsulated within N doped HCS (NHCS).[6] Typitally, the synthesis requires the employment of an easily removable material (e.g., SiO_2) as the hard template for the coating and subsequent pyrolysis of nitrogen containing precursors (e.g., dopamine, and resorcinol–formaldehyde) to afford a N-rich carbon shell.[7] Then NHCS could be obtained after the removal of siliceous components by treatment with HF solution, which is then used as supports for the immobilization of metal NPs by impregnation or coprecipitation. Although this traditional synthetic route has been widely used, it involves tedious and complicated steps, and requires hazardous reagents (i.e., HF) for the removal of hard templates and excess reducing reagents for the reduction of metal precursors. Moreover, postloading of metal NPs to the support would lead to insufficient attachment of the NPs to the support.[3c] Therefore, it is highly desirable to develop a simple and efficient strategy to integrate metal NPs into NHCS for the design of advanced nanocatalysts.

Recently, solid-state pyrolysis of porous organic networks, such as metal-organic frameworks (MOFs)[8] and covalent organic frameworks (COFs),[9] has emerged as a simple, efficient and promising approach for the fabrication of nanostructured materials. Especially, COFs are only composed of organic skeletons, making them outstanding templates for facile preparation of porous carbons.[10] By carefully choosing construction units, COFs with various morphographies and functions could be synthesized, thus allowing to control the shape and composite of the final nanostructured materials via thermolysis.[11] Nevertheless, to the best of our knowledge, the employment of COF-based materials as pyrolysis sacrificial precursors for NHCS supported metal NPs composites has never been explored.

[a] Key Laboratory of Fuel Cell Technology of Guangdong Province, School of Chemistry and Chemical Engineering, South China University of Technology, Guangzhou 510640 (China), E-mail: liyw@scut.edu.cn
[b] Departamento de Química Orgánica, Universidad de Córdoba, Edif. Marie Curie, Ctra Nnal IV-A, Km 396, E14014, Córdoba (Spain), E-mail: q62alsor@uco.es
Electronic Supplementary Information (ESI) available: Experimental details and catalysts characterization. See DOI: 10.1039/x0xx00000x

View Article Online
DOI: 10.1039/C6SC01659F

In this work, we report a novel one-step synthesis strategy for in-situ fabrication of NHCS encapsulated metal NPs by using metal ion doped COF as precursor. As a proof of concept, we chose LZU1,[12] a hollow spheric COF, as the NHCS template. In this COF, the eclipsed nitrogen atoms in adjacent layers can serve as coordination sites for transition cations such as Pd^{2+} (Scheme 1). During the annealing process under an inert atmosphere, Pd cations will be reduced to form Pd NPs, meanwhile the N-containing organic linkers will serve as both carbon and nitrogen sources for the formation of NHCS. Through this rational design, the high nitrogen doping in the NHCS support could geometrically and electronically modify the in-situ growth of Pd NPs and the hollow structure could facilitate the diffusion of substrate, endowing the obtained material with superior catalytic capability. As demonstrated in the hydrogenation of nitrobenzene and oxidation of cinnamyl alcohol, this unique Pd@NHCS hybrid material exhibits significantly improved catalytic performances in terms of activity and selectivity as copmpared to the Pd/N-C and commercial Pd/C catalysts under identical conditions.

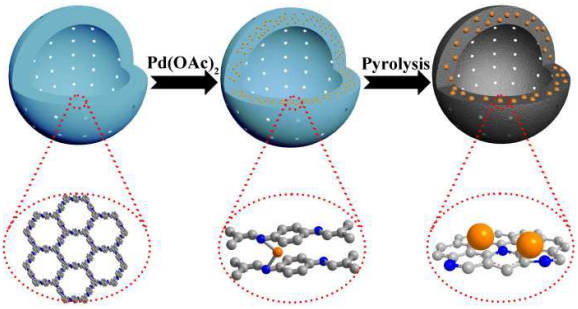

Scheme 1. Schematic illustration of the fabrication of Pd@NHCS. Color coding: grey, carbon; blue, nitrogen; orange, Pd precursors or NPs.

Results and discussion

LZU1 was synthesized following a previously reported protocol with slight modifications.[12] Pd(II)-doped LZU1 (Pd^{II}-LUZ1) was facilely prepared through a simple impregnation of LZU1 with palladium acetate. Field emissions canning electron microscopy (FESEM) and transmission electron microscope (TEM) images show that Pd^{II}-LZU1 is mainly composed of hollow spheres with a diameter of about 250 nm and a shell thickness of ca. 40 nm (Figure S1a, and Figure 1a-b). X-ray photoelectron spectroscopy (XPS) measurements were performed to investigate the intermolecular interaction between the COF and $Pd(OAc)_2$. For the Pd 3d 5/2 spectrum, one peak at 337.8 eV was observed for Pd^{II}-LZU1, characteristic of divalent Pd ions (Figure S2). This value shifts negatively in comparison with that of free $Pd(OAc)_2$.[13] In addition, the parent LZU1 contains only one kind of N, i.e., Schiff base nitrogen (Figure 2a). After the immobilization of $Pd(OAc)_2$, a new N 1s peak at ca. 400 eV was observed. The shift of the N 1s peak toward a higher binding energy reflects a decrease in the electron density of N. These results indicate that there exists a strong coordination between $Pd(OAc)_2$ with the imine groups of LZU1.

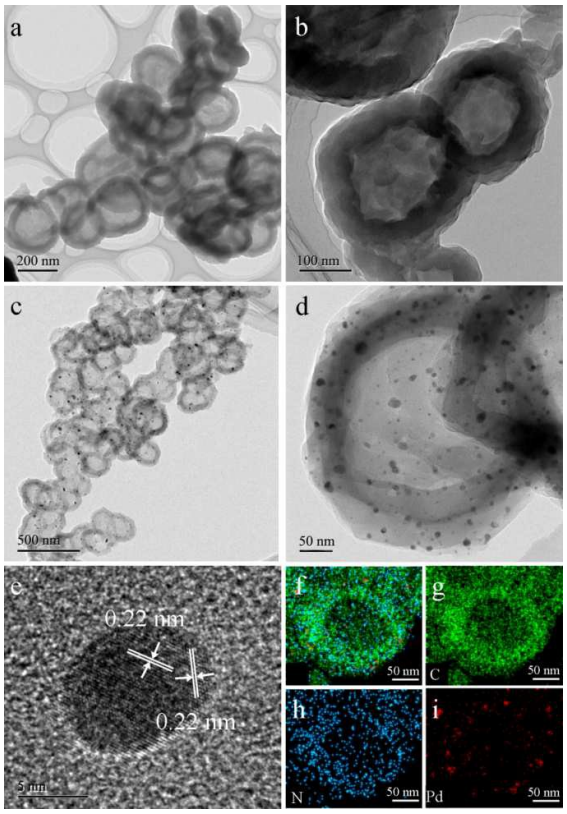

Figure 1. (a-b) TEM images of Pd^{II}-LUZ1. (c-d) TEM images of Pd@NHCS(500). (e) HRTEM image of Pd NPs. (f-i) EDS elemental mapping of a Pd@NHCS(500) particle (green: C; blue: N and red: Pd).

As observed from the thermogravimetric analysis (TGA) curves (Figure 3a), Pd^{II}-LZU1 begins to decompose when the temperature is increased to ca. 500 °C under argon. Therefore, the Pd^{II}-LZU1 composites were annealed at 500 °C for 3 h with a heating rate of 1 °C/min to produce the final composites, which is denoted as Pd@NHCS(500). The carbonized products show similar morphology as compared to the precursor (Figure S1b). The diameter of the spheres and the thickness of the shell measured from the TEM images are ca. 200 nm and 30 nm, respectively (Figure 1c-d). The observed smaller particles in comparison with the precursors are reasonable as a consequence of volume shrinking after high-temperature heating. The corresponding dark field scanning transmission electron microscopy (DFSTEM) images (Figure S3) clearly show hollow shells. The Pd NPs are uniformly distributed with an average size of 6 nm, mostly located within the carbon shell. A representative high-resolution TEM image of Pd-in-UiO-67 displays distinct lattice fringes with d spacings of 0.22 nm, corresponding to the (111) lattice spacing of face-centered cubic Pd (Figure 1e). The surface of Pd is not coated by carbon layers, indicating that Pd NPs are embedded within the pores or supported on the surface of NHCS, thus accessible to the reactants. The energy dispersive spectrometer (EDS) mapping

View Article Online
DOI: 10.1039/C6SC01659F

images (Figure 1f-i) reveal the uniform distribution of C, N and Pd elements all over the support. The Pd content in the Pd@NHCS(500) is 2.4 wt% as measured by atomic absorption spectroscopy (AAS). Elemental analysis results further reveal that Pd@NHCS(500) is composed of C, H and N elements, and the nitrogen content is as high as 11.0 wt% (Table S1).

Futher increasing the annealing temperature to 600 °C, some particles with a broken outer shell were observed (Figure S4). The as-formed Pd NPs show some aggregation, with an average size of 19 nm. Elevating the annealing temperatures also leads to a decrease in nitrogen content wihile an increase in Pd content of the resultant samples (Table S1).

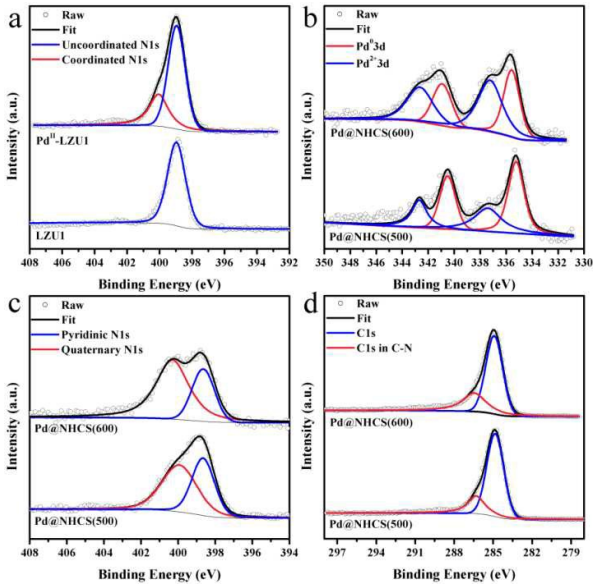

Figure 2. (a) XPS N 1s of LUZ1 before and after the immobilization of $Pd(OAc)_2$. High-resolution (b) Pd 3d spectra, (c) N1s spectra, and (d) C1s spectra for Pd@NHCS(500) and Pd@NHCS(600).

The crystalline phases and structures of the materials were examined by powder X-ray diffraction (XRD) and Raman analysis. The characteristic XRD peaks (Figure 3b) at 40.1, 46.7, 68.2, 82.2 and 86.7 may be assigned to the (111), (200), (220), (311) and (222) reflections of Pd (JCPDS 65-6174), respectively. No peaks for other possible impurity were detected, indicating high purity of the synthesized materials. Increasing the calcination temperature enhances the intensity of the Pd diffraction peak, suggesting a bigger size and higher crystallinity degree of Pd NPs as the calcination temperature increases, which is in good agreement with that observed in TEM analysis. A broad and weak XRD peak around 29.5° was detected (Figure 3b), confirming the existence of amorphous carbon. In addition, the Raman spectra show two broad bands (Figure 3d), in which the G band at ~1584 cm^{-1} indicates the in-plane vibration of aromatic carbon atoms, while the D band at ~1313 cm^{-1} is a disorder induced Raman feature caused by the nonperfect crystalline structure.[14] The relative ratio of D band to G band (I_D/I_G) in the Raman spectra of Pd@NHCS(500) and Pd@NHCS(600) is 1.30 and 1.16, respectively. The D band appears to be stronger than the G band, implying the generation of large amounts of defects because of the high nitrogen doping percentage in the resulting composites.

N_2 adsorption–desorption experiments were performed at 77 K to measure the surface area and porosity of the resultant NHCS supported Pd composites. The adsorption/desorption isotherms are shown in Figure 3c. Pd@NHCS samples show a typical adsorption curve of type I plus IV with steep increases at low relative pressures and an obvious hysteresis loop in the P/P_0 range of 0.8–1, revealing the presence of micro-, meso- and macropores. These Pd@NHCS materials have Brunauer–Emmett–Teller (BET) surface areas of 450–550 m^2 g^{-1} and pore volumes of 0.19–0.24 cm^3 g^{-1} (Table S2). The porous structure of NHCS supports would benefit the transportation of molecules to embeded Pd NPs in catalytic transformations.

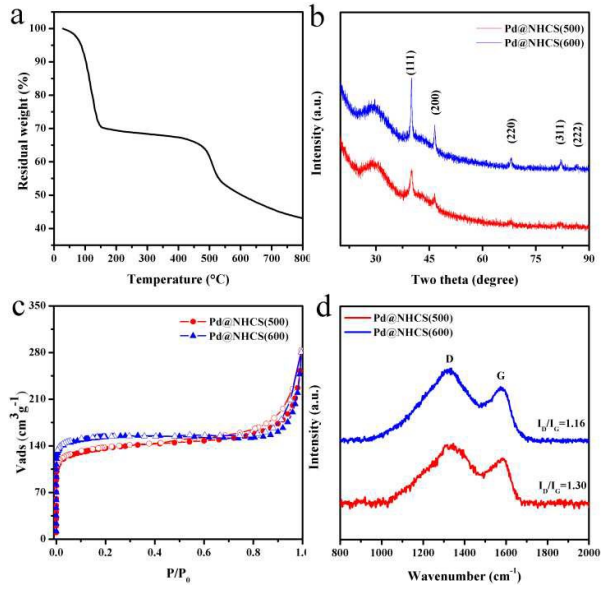

Figure 3. (a) TGA curve of Pd^{II}-LUZ1. (b) Powder XRD patterns for Pd@NHCS(500) and Pd@NHCS(600). (c) Nitrogen adsorption isotherms for Pd@NHCS(500) and Pd@NHCS(600). (d) Raman spectra for Pd@NHCS(500) and Pd@NHCS(600).

XPS measurements were conducted to investigate the electronic and structural properties of Pd@NHCS composites. As illustrated in Figure 2b, Pd@NHCS(500) contains ca. 60% Pd^0 as revealed by the Pd 3d 5/2 XPS peaks at 335.2 and 337.4 eV, relatively a less percentage of Pd^0 (ca. 43%) was observed for Pd@NHCS(600). The N 1s spectra of the Pd@NHCS composites can be deconvoluted into two peaks at 398.6 and 399.9 eV, respectively, which are consistent with pyridinic N and quaternary N in the carbon texture (Figure 2c). The ratio of graphitic nitrogen to pyridinic nitrogen in Pd@NHCS is increased when the pyrolysis temperature is enhanced (e.g., 1.3 for 500 °C and 2.2 for 600 °C), implying a higher graphitization degree at elevated temperatures. The C 1s XPS spectra of the Pd@NHCS composites present in Figure 2d can be deconvoluted into two major peaks. The peak at 284.6 eV corresponds to the sp^2 graphitic carbon species, while the other one at 285.4 eV may be assigned to the sp^2-carbon

View Article Online
DOI: 10.1039/C6SC01659F

containing nitrogen atoms, suggesting the presence of nitrogen functionalities on the surface of NHCS.

The catalytic efficiencies of the as-synthesized nanohybrid materials were evaluated using the hydrogenation of nitrobenzene to aniline as model reaction.[15] The reactions were performed under atmospheric pressure of H_2 and room temperature (25 °C), and the reaction profiles are shown in Figure 4. It was found that hydrogenation of nitrobenzene in alcohols would afford not only aniline, but also imine, N-ethylaniline and tertiary amine as by-products coming from the further N-alkylation of amine with alcohol.[16] Pure NHCS(500) gave essentially no conversion under the reaction condition, implying the need of a metal to perform the hydrogenation of nitrobenzene. Pd@NHCS(500) showed a very high activity with a complete conversion of nitrobenzene and 88% aniline selectivity within only 50 min. Pd@NHCS(600) was less active than Pd@NHCS(500), requiring a much longer time (ca. 100 min) to obtain a quantitative conversion of nitrobenzene. The relatively poor performance may result from the larger particle size of Pd NPs in Pd@NHCS(600) (as demonstrated by the TEM analysis). Nevertheless, the Pd@NHCS(600) catalyst could also achieve a similar high selectivity to aniline as Pd@NHCS(500) (Figure 4b).

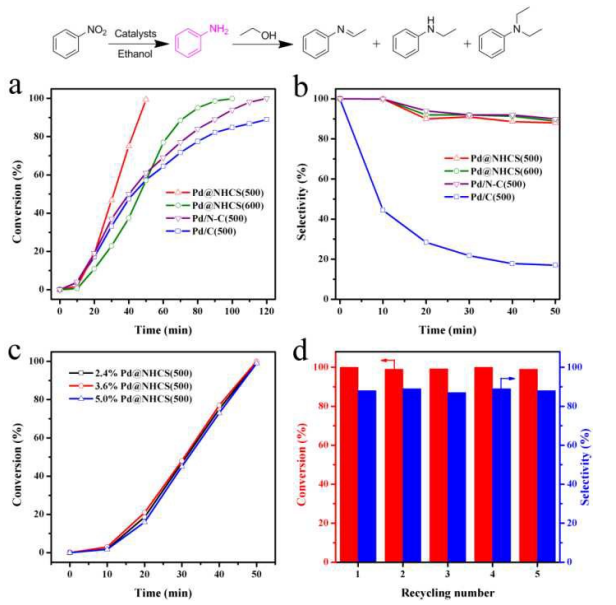

Figure 4. (a) Nitrobenzene conversions and (b) selectivities to aniline versus time in the hydrogenation of nitrobenzene over the Pd@NHCS(500), Pd@NHCS(600), Pd/C-N(500) and Pd/C(500). (c) Effect of Pd loading on the catalytic performance of Pd@NHCS(500). (d) Recyclability of 2.4% Pd@NHCS(500) in the hydrogenation of nitrobenzene.

To illustrate the benefit of the hollow spheric structure and N dopant to the catalytic performance, we also prepared Pd NPs supported on N doped carbon and commercial carbon materials for comparison. First, N doped carbon was prepared according to our previous report.[17] The N-C material was then impregnated with $Pd(OAc)_2$ and treated at 500°C for 3 h under argon. The resulting material is denoted as Pd/N-C(500). TEM image shows that Pd/N-C(500) has a comparable average size of Pd NPs to that of Pd@NHCS(500) (Figure S5a). AAS analysis demonstrated that Pd/N-C(500) had a similiar Pd loading (2.1 wt%) to that of Pd@NHCS(500). In the hydrogenation of nitrobenzene, Pd/N-C(500) exhibited a moderate activity and produced aniline in 89% yield in 120 min. The substantially lower catalytic activity for Pd/N-C(500) as compared to Pd@NHCS(500) indicates that the hollow structure and porous shell of the NHCS may facilitate the substrate to access Pd NPs thus showing an enhanced reactivity.

On the other hand, $Pd(OAc)_2$ was impregnated onto a commercial carbon followed by annealing at 500 °C for 3h to afford Pd/C(500). Under the similar reaction conditions, Pd/C(500) showed the worst activity, giving only 89% conversion in 120 min. Interestingly, Pd/C(500) exhibited a different product distribution comparing with those of Pd@NHCS and Pd/N-C. As shown in Table S3, the selectivity to aniline was very low (12%), while mono- or di-N-alkylation product became the main product over the Pd/C(500) catalyst. To gain more in-depth information about the different catalytic behaviors, the Pd@NHCS(500) and Pd/C(500) materials were characterized by TEM, AAS and XPS. The as-prepared Pd NPs in Pd/C(500) have a similar size distribution, Pd loading (2.0 wt%) and percentage of Pd^0 as that of Pd@NHCS(500) (Figures S5b and S6). However, interestingly, the binding energy of Pd 3d is shifted to a higher value by approximately 0.5 eV. This could be due to the lack of electron donating dopant (e.g., N) in the carbon support, resulting in more positively charged Pd NPs on the Pd/C(500).

In situ attenuated total reflection infrared (ATR-IR) spectroscopy was further employed to gain some molecular insights into the surface adsorption property of the catalysts for ethanol. Initially, N_2-saturated ethanol adsorption on different catalyst surfaces was investigated. The difference spectra of adsorbed ethanol on Pd@NHCS(500) is displayed in Figure S7. In this plot, spectrum of the pristine Pd@NHCS(500) (Figure S8) was subtracted. Bands located in the region of 1200–1500 cm^{-1} are characteristics of C–H stretchings for methyl and methylene groups in ethanol.[18] These bands show no obvious change in intensity with time, implying a weak absorption of ethanol on the Pd@NHCS(500) material. However, for Pd/C(500), these bands gradually become weaker with time, suggesting that ethanol might adsorb strongly on the Pd/C(500). Nitrogen functionalities on NHCS could act as coordination donor ligands to tune the electronic properties of Pd NPs to exhibited a comparatively higher negative charge to that of Pd/C(500) (Figure S6). Considering alcohols may be adsorbed on the Pd surface via the lone electron pair of the oxygen atom, electron-enriched Pd in Pd@NHCS(500) may depress the adsorption of ethanol while positively charged Pd in Pd/C(500) facilitates this adsorption.[19] Therefore, it is reasonable that ethanol could undergo N-alkylation with aniline when using Pd/C(500) as catalyst, while the alkylation reaction is supressed over the Pd@NHCS(500) catalyst.

The proposed protocol could be applied for the preparation of Pd@NHCS with different Pd loadings, simply by changing the impregnated amounts of $Pd(OAc)_2$ on COFs. As measured by AAS, we could achieve different Pd loadings (e.g., 2.4%,

View Article Online
DOI: 10.1039/C6SC01659F

3.6% and 5.0%) on NHCS. As shown in Figure S9, these samples showed comparable size distribution of Pd NPs. These composites show similar catalytic activities for nitrobenzene hydrogenation when a same amount of Pd (1 mol% to substrate) was used, indicating the loading of Pd on NHCS would not play a critical role in the activity (Figure 4c).

The stability and reusability are of great importance for the practical application of a heterogeneous catalyst. After reaction, the catalyst was separated by centrifugation. AAS analysis of the reaction solution showed that the concentration of palladium in solution was below the detection limit, suggesting that the leaching of active Pd during the reaction was negligible. The used catalyst was thoroughly washed with ethanol, and then dried under vacuum to remove the residual solvent. Results included in Figure 4d reveals that Pd@NHCS(500) could be regenerated and reused at least five times in the subsequent reactions without significant lose of catalytic activity and selectivity. The metal contents of the reused catalysts are almost the same as the fresh one, as determined by AAS. TEM images also show that no apparent Pd aggregation could be observed on the recycled catalysts (Figure S10). These results demonstrate that the highly active Pd@NHCS(500) catalyst is stable and reusable under the investigated conditions.

Encouraged by these promising results, we further examined the catalytic activity of these Pd catalysts in the aerobic oxidation of cinnamyl alcohol. The reactions were carried out at 80 °C under air atmosphere and base-free conditions. As shown in Table S4, compared with Pd/C-N(500) and Pd/C(500), Pd@NHCS(500) exhibited the highest catalytic activity, which provided a quantitative conversion of cinnamyl alcohol into cinnamyl aldehyde within 10 h. These results can further support the conclusion that porous hollow spheric structures, highly dispersed Pd NPs and uniform distribution of N dopants contribute to achieving superior catalytic activities.

Conclusions

In summary, we have demonstrated a novel and facile in-situ strategy to synthesize metal NPs encapsulated in the shell of nitrogen doped hollow carbon spheres (NHCS) by using metal ions doped COFs as the precursors through a simple annealing process. The obtained Pd@NHCS composites exhibit unprecedent catalytic performances in terms of activity and selectivity that are much superior to conventional Pd/N-C and commercial Pd/C catalysts in the hydrogenation of nitrobenzene and oxidation of cinnamyl alcohol. The obtained excellent catalytic properties should be originated from the synergism of porous hollow spheric structure, highly dispersed Pd NPs, and uniform distribution of N dopants. This proposed protocol can simplify the synthesis process with the elimination of hard templates and significant reduction of wastes as compared to other conventional methodologies, which might be extended to the preparation of other metal NPs@NHCS composites for potential applications in a variety of fields including heterogeneous catalysis demonstrated here.

Acknowledgements

This work was supported by the NSF of China (21322606, 21436005, and 21576095), the Doctoral Fund of Ministry of Education of China (20120172110012), Fundamental Research Funds for the Central Universities (2015ZP002 and 2015PT004), and the Guangdong NSF (2013B090500027).

Notes and references

1 (a) Y. Li, J. Shi, *Adv. Mater.*, 2014, **26**, 3176; (b) J. Qi, X. Lai, J. Wang, H. Tang, H. Ren, Y. Yang, Q. Jin, L. Zhang, R. Yu, G. Ma, Z. Su, H. Zhao, D. Wang, *Chem. Soc. Rev.*, 2015, **44**, 6749; (c) Y. Chen, H. R. Chen, J. L. Shi, *Acc. Chem. Res.* 2014, **47**, 125; (d) Z. Wang, L. Zhou, X. W. Lou, *Adv. Mater.*, 2012, **24**, 1903; (e) J. Chen, D. Wang, J. Qi, G. Li, F. Zheng, S. Li, H. Zhao, Z. Tang, *Small*, 2015, **11**, 420.

2 (a) J. Liu, N. P. Wickramaratne, S. Z. Qiao, M. Jaroniec, *Nat. Mater.*, 2015, **14**, 763; (b) A. D. Roberts, X. Li, H. Zhang, *Chem. Soc. Rev.*, 2014, **43**, 4341.

3 (a) G. H. Wang, J. Hilgert, F. H. Richter, F. Wang, H. J. Bongard, B. Spliethoff, C. Weidenthaler, F. Schüth, *Nat. Mater.*, 2014, **13**, 293; (b) Y. J. Hong, Y. C. Kang, *Small*, 2015, **11**, 2157; (c) C. Baldizzone, S. Mezzavilla, H. W. P. Carvalho, J. C. Meier, A. K. Schuppert, M. Heggen, C. Galeano, J. D. Grunwaldt, F. Schüth, K. J. J. Mayrhofer, *Angew. Chem. Int. Ed.*, 2014, **53**, 14250; (d) H. Liu, Z. Feng, J. Wang, L. Zhang, D. Su, *Catal. Today*, 2016, **260**, 55.

4 (a) M. Zhao, K. Deng, L. He, Y. Liu, G. Li, H. Zhao, Z. Tang, *J. Am. Chem. Soc.*, 2014, **136**, 1738; (b) X. Liu, L. He, J. Zheng, J. Guo, F. Bi, X. Ma, K. Zhao, Y. Liu, R. Song, Z. Tang, *Adv. Mater.*, 2015, **27**, 3273.

5 (a) S. Y. Kim, H. M. Jeong, J. H. Kwon, I. W. Ock, W. H. Suh, G. D. Stucky, J. K. Kang, *Energy Environ. Sci.*, 2015, **8**, 188; (b) Y. Jiao, Y. Zheng, M. Jaroniec, S. Z. Qiao, *J. Am. Chem. Soc.*, 2014, **136**, 4394; (c) J. Duan, S. Chen, M. Jaroniec, S. Z. Qiao, *ACS Catal.*, 2015, **5**, 5207; (d) J. Y. Cheon, J. H. Kim, J. H. Kim, K. C. Goddeti, J. Y. Park, S. H. Joo, *J. Am. Chem. Soc.*, 2014, **136**, 8875; (e) A. Primo, F. Neatu, M. Florea, V. Parvulescu, H. Garcia, *Nat. Commun.*, 2014, **5**, 5291; (f) S. Navalon, A. Dhakshinamoorthy, M. Alvaro, H. Garcia, *Chem. Rev.*, 2014, **114**, 6179.

6 a) R. Liu, S. M. Mahurin, C. Li, R. R. Unocic, J. C. Idrobo, H. Gao, S. J. Pennycook, S. Dai, *Angew. Chem. Int. Ed.*, 2011, **50**, 6799; b) H. Wang, X. Bo, A. Wang, L. Guo, *Electrochem. Commun.*, 2013, **36**, 75; c) C. Galeano, J. C. Meier, M. Soorholtz, H. Bongard, C. Baldizzone, K. J. J. Mayrhofer, F. Schüth, *ACS Catal.*, 2014, **4**, 3856.

7 a) S. Feng, W. Li, Q. Shi, Y. Li, J. Chen, Y. Ling, A. M. Asiri, D. Zhao, *Chem. Commun.*, 2014, **50**, 329; b) D. Zhou, L. Yang, L. Yu, J. Kong, X. Yao, W. Liu, Z. Xu, X. Lu, *Nanoscale*, 2015, **7**, 1501.

8 (a) W. Xia, A. Mahmood, R. Zou, Q. Xu, *Energy Environ. Sci.*, 2015, **8**, 1837; (b) Y. Chen, C. Wang, Z. Wu, Y. Xiong, Q. Xu, S. Yu, H. Jiang, *Adv. Mater.*, 2015, **27**, 5010; (c) S. Zhao, H. Yin, L. Du, L. He, K. Zhao, L. Chang, G. Yin, H. Zhao, S. Liu, Z. Tang, *ACS Nano*, 2014, **8**, 12660; (d) H. Liu, S. Zhang, Y. Liu, Z.Yang, X. Feng, X. Lu, F. Huo, *Small*, 2015, *11*, 3130; (e) F. Zheng, M. He, Y. Yang, Q. Chen, *Nanoscale*, 2015, **7,** 3410; (f) L. Zhang, H. B. Wu, X. W. Lou, *J. Am. Chem. Soc.*, 2013, **135**, 10664.

9 (a) N. Kang, J. H. Park, J. Choi, J. Jin, J. Chun, I. G. Jung, J. Jeong, J. G. Park, S. M. Lee, H. J. Kim, S. U. Son, *Angew. Chem. Int. Ed.*, 2012, **51**, 6626; (b) P. Pachfule, V. M. Dhavale, S. Kandambeth, S. Kurungot, R. Banerjee, *Chem. Eur. J.*, 2013, **19**, 974; (c) Z. Hu, J. Jiang, *Nanoscale*, 2014, **6**, 772.

10 (a) J. K. Sun, Q. Xu, *Energy Environ. Sci.*, 2014, **7**, 2071; (b) X. Liu, L. Zhou, Y. Zhao, L. Bian, X. Feng, Q. Pu, *ACS Appl. Mater.*

View Article Online
DOI: 10.1039/C6SC01659F

Interfaces, 2013, **5**, 10280; (c) D. Zhu, L. Li, J. Cai, M. Jiang, J. Qi, X. Zhao, *Carbon*, 2014, **79**, 544.
11 Z. S. Wu, L. Chen, J. Liu, K. Parvez, H. Liang, J. Shu, H. Sachdev, R. Graf, X. Feng, K. Müllen, *Adv. Mater.*, 2014, **26**, 1450.
12 S. Y. Ding, J. Gao, Q. Wang, Y. Zhang, W. G. Song, C. Y. Su, W. Wang, *J. Am. Chem. Soc.*, 2011, **133**, 19816.
13 (a) G. Q. Kong, S. Ou, C. Zou, C. D. Wu, *J. Am. Chem. Soc.*, 2012, **134**, 19851; (b) L. Chen, X. Chen, H. Liu, C. Bai, Y. Li, *J. Mater. Chem. A*, 2015, **3**, 15259; (c) L. Chen, Z. Gao, Y. Li, *Catal. Today*, 2015, **245**, 122.
14 X. Xu, Y. Li, Y. Gong, P. Zhang, H. Li, Y. Wang, *J. Am. Chem. Soc.*, 2012, **134**, 16987.
15 (a) L. Chen, H. Chen, R. Luque, Y. Li, *Chem. Sci.*, 2014, **5**, 3708; (b) L. Chen, X. Chen, H. Liu, Y. Li, *Small*, 2015, **11**, 2642; (c) F. A. Westerhaus, R. V. Jagadeesh, G. Wienhöfer, M. M. Pohl, J. Radnik, A. E. Surkus, J. Rabeah, K. Junge, H. Junge, M. Nielsen, A. Brückner, M. Beller, *Nat. Chem*., 2013, **5**, 537; (d) A. Corma, P. Serna, *Science*,2006, **313**, 332.
16 (a) C. Tang, L. He, Y. Liu, Y. Cao, H. He, K. Fan, *Chem. Eur. J.*, 2011, **17**, 7172; (b) Y. Shiraishi, M. Ikeda, D. Tsukamoto, S. Tanaka, T. Hirai, *Chem. Commun.*, 2011, **47**, 4811; (c) X. Cui, Y. Deng, F. Shi, *ACS Catal.*, 2013, **3**, 808.
17 W. Zhong, H. Liu, C. Bai, S. Liao, Y. Li, *ACS Catal.*, 2015, **5**, 1850.
18 S. W. Ho, Y. S. Su, *J. Catal.*, 1997, **168**, 51.
19 (a) R. M. Souto, J. L. Rodríguez, E. Pastor, *Langmuir*, 2000, **16**, 8456; (b) Y. Shiraishi, K. Fujiwara, Y. Sugano, S. Ichikawa, T. Hirai, *ACS Catal.*, 2013, **3**, 312; (c) C. Keresszegi, D. Ferri, T. Mallat, A. Baiker, *J. Phys. Chem. B*, 2005, **109**, 958.